Two-Photon Absorption Properties of Two-Dimensional π-Conjugated Chromophores: Combined Experimental and Theoretical Study

Koji Ohta,* Satoru Yamada,[†] and Kenji Kamada

Research Institute for Ubiquitous Energy Devices, National Institute of Advanced Industrial Science and Technology (AIST), 1-8-31 Midorigaoka, Ikeda, Osaka 563-8577, Japan

Aaron D. Slepkov[‡] and Frank A. Hegmann

Department of Physics, University of Alberta, Edmonton, Alberta T6G 2G7, Canada

Rik R. Tykwinski

Institut für Organische Chemie, Friedrich-Alexander-Universität Erlangen-Nürnberg, Henkestrasse 42, D-91054 Erlangen, Germany

Laura D. Shirtcliff and Michael M. Haley

Department of Chemistry and Materials Science Institute, University of Oregon, Eugene, Oregon 97403-1253, United States

Paweł Sałek, Faris Gel'mukhanov, and Hans Ågren

Department of Theoretical Chemistry, School of Biotechnology, Royal Institute of Technology, SE-10691 Stockholm, Sweden

The two-photon absorption (TPA) properties of four TPEB [tetrakis(phenylethynyl)benzene] derivatives (**TD**, **para**, **ortho**, and **meta**) with different donor/acceptor substitution patterns have been investigated experimentally by the femtosecond open-aperture Z-scan method and theoretically by the time-dependent density-functional theory (TDDFT) method. The four compounds show relatively large TPA cross sections, and the all-donor substituted species (**TD**) displays the largest TPA cross-section $\sigma^{(2)} = 520 \pm 30$ GM. On the basis of the calculated electronic structure, **TD** shows no TPA band in the lower energy region of the spectrum because the transition density is concentrated on particular transitions due to the high symmetry of the molecular structure. The centrosymmetric donor−acceptor TPEB **para** shows excitations resulting from transitions centered on D−π−D and A−π−A moieties, as well as transition between the D−π−D and A−π−A moieties; this accounts for the broad nature of the TPA bands for this compound. Calculations for two noncentrosymmetric TPEBs (**ortho** and **meta**) reveal that the diminished TPA intensities of higher-energy bands result from destructive interference between the dipolar and three-state terms. The molecular orbitals (MOs) of the TPEBs are derivable with linear combinations of the MOs of the two crossing BPEB [bis(phenylethynyl)benzene] derivatives. Overall, the characteristics of the experimental spectra are well-described based on the theoretical analysis.

1. Introduction

Over the past decade, two-photon absorption (TPA) has re-emerged not only as an interesting spectroscopic phenomena but also as a process that can be harnessed to provide for technologically useful applications such as 3D-microfabrication and fluorescence imaging.[1] The evolution of molecular design to increase TPA cross sections, $\sigma^{(2)}$, has in many ways mirrored the analogous evolution of organic chromophores for other nonlinear optical (NLO) processes. It started with relatively simple one-dimensional, conjugated molecules (−π−) appended with electron-donating (D) and/or electron-withdrawing sub-

stituents (A).[1] This provided several possible molecular arrangements (e.g., D−π−D, D−π−A, D−A−D, A−D−A), but all conjugation pathways were unidirectional. Molecular design then evolved into more complex structural motifs that often incorporated multidimensional conjugation pathways that featured numerous conjugated circuits between donor and acceptor substituents.[2] As such, there are now many examples of TPA-active molecules with two- or three-dimensional frameworks. Most recently, for example, Rumi and co-workers have shown that the TPA cross sections for all donor and donor−acceptor tetrastyrylbenzenes (TSBs, Figure 1) and analogous tetrastyrylpyrazene (not shown) do not benefit from the presence of two-dimensional conjugation in comparison to their linearly conjugated analogues.[3] Tao and co-workers, on the other hand, indicate that TPA properties are enhanced by terminating TSBs with *N,N*-diethyl- and *N,N*-dibutylaniline groups,[4] but given that
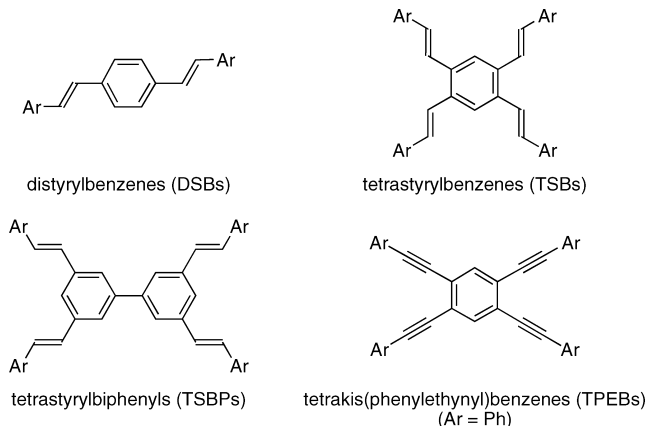
Figure 1. Molecular structures of DSBs, TSBs, TSBPs, and TPEBs.

the TPA cross-section values reported in this latter study are in line with those of Rumi et al.,[3] it seems likely that the 2D framework was not necessarily beneficial. A similar finding was reported for TSBs terminated with pyridyl groups, whereby two-dimensional conjugation brought about little enhancement in $\sigma^{(2)}$.[5] Ma and Yang have explored TPA for tetrastyrylbiphenyl (TSBP) terminated with *N,N*-diphenylaniline groups, in both solution and solid state.[6] They, however, find a TPA cross-section for the two-dimensional TSBP that is three times that of the linear DSB analogue, and values in the solid state for TSBP are over 6-fold higher than for the corresponding DSB derivative.[7,8] Up to the present date, the TPA studies for molecular materials have been extended to compounds having multidimensional structures including purely organic and organometallic compounds such as porphyrins.[9]

Our own investigations of two-dimensional chromophores[10,11] have centered on an alternative structural platform, that of the tetra(arylethynyl)benzene (TPEB) framework. Our recent NLO work used the ultrafast Z-scan method to compare the TPA properties of a pair of quadrupolar D/A TPEB chromophores, **TD** and **para** (shown in Figure 2).[12] The all-donor substituted species (**TD**) displays a peak TPA cross-section $\sigma^{(2)} = 520 \pm 30$ GM that is more than twice that of the D−A species (**para**) $\sigma^{(2)} = 240 \pm 20$ GM. Given the increasing general importance of optimizing TPA systems, coupled with the unclear picture of how multidimensional chromophores might lead to enhanced TPA performance, we sought to elucidate the mechanisms of TPA cross sections for TPEB derivatives through time-dependent density-functional theory (TDDFT) methods. The results of this study are reported herein through comparisons to our experimental results.

2. Methods

2.1. Experimental Method. TPEBs used in the present study were prepared according to the procedure previously described in the literature.[10]

One-photon absorption (OPA) spectra of TPEBs dissolved in tetrahydrofuran (THF) were recorded with a UV−vis spectrophotometer (Shimadzu UV3150). TPA spectra in THF (5−11 mM) were obtained with the open-aperture Z-scan method using a femtosecond optical parametric amplifier pumped with Ti:sapphire regenerate amplifier system (Spectra-Physics OPA-800 and Spitfire) operating at a 1 kHz repetition rate. Typical duration of the output pulses was 125 fs. The Rayleigh range of the Z-scan setup was 4−8 mm, depending on wavelength, and was longer than the 1-mm cuvette optical

path length *L*, satisfying the thin sample condition.[13] The details of this setup have been reported elsewhere.[14] Open-aperture traces were measured as a function of different incident powers (corresponding to the peak on-axis optical intensities, I_0, in the range of 10−150 GW/cm^2) for each sample and wavelength. The recorded traces were analyzed by curve fitting to a model function by assuming the simultaneous TPA process induced by an optical pulse having the Gaussian profiles in time and space.[15] From each curve fitting, the two-photon absorbance $q_0 = \sigma^{(2)} I_0 L N_c / \hbar \omega$ was obtained, where $\sigma^{(2)}$ is the TPA cross sections, N_c is number density of the sample, and $\hbar \omega$ is the photon energy. Good linearity was found for q_0 against the incident power (therefore against I_0) at each wavelength, showing that contributions from the excited-state absorption previously reported at a longer time scale for these systems[12] was negligible under the present measurement conditions.[16] MPPBT[15] and l,4-bis(*p*-dibutylaminostyryl)-2,5-dimethoxybenzene (compound **8** in ref 17) were measured under the same experimental conditions as references for confirmation of the absolute $\sigma^{(2)}$ values reported here.

2.2. Calculation Method. For the theoretical simulations of OPA spectra, the same equations used previously[18] are used for calculating the molar absorption coefficient $\varepsilon(\omega)$.

$$\varepsilon(\omega) = \frac{10^{-3}}{\ln 10} N_A \frac{4\pi^2 \omega}{c\hbar n} \langle |\mathbf{M}_{fg}|^2 \rangle g(\omega) \qquad (1)$$

where N_A is Avogadro's number, ω is the angular frequency of the incident light in s^{-1}, *n* is the refractive index of the sample, and $g(\omega)$ is the normalized spectral shape function. $\mathbf{M}_{fg}$ is the transition moment between the ground (*g*) and excited (*f*) states. By adopting the usual dipole approximation, $\mathbf{M}_{fg}$ is expressed by the matrix element of the dipole moment operator as

$$\mathbf{M}_{fg} = \langle f | \vec{\varepsilon} \cdot \vec{\mu} | g \rangle \qquad (2)$$

where $\vec{\varepsilon}$ is the unit vector along the polarization direction of the incident light and $\vec{\mu}$ is the dipole moment operator. In the present spectral simulation, the following Lorentzian function is used as the normalized shape function $g(\omega)$.

$$g(\omega) = \frac{1}{\pi} \frac{\Gamma_{fg}}{(\omega_{fg} - \omega)^2 + \Gamma_{fg}^2} \qquad (3)$$

where Γ_{fg} is the damping constant in s^{-1}.

The TPA cross-section spectrum $\sigma^{(2)}(\omega)$ for the case of single-beam experiments is expressed as

$$\sigma^{(2)}(\omega) = \frac{4\pi^3 \omega^2}{c^2 n^2} \langle |\mathbf{M}_{fg}^{(2)}|^2 \rangle g(2\omega) \qquad (4)$$

where $\mathbf{M}_{fg}^{(2)}$ is the two-photon transition matrix element having the same dimension as the dipole polarizability, expressed as

$$\mathbf{M}_{fg}^{(2)} = \frac{2}{\hbar} \sum_k \frac{\langle f | \vec{\varepsilon} \cdot \vec{\mu} | k \rangle \langle k | \vec{\varepsilon} \cdot \vec{\mu} | g \rangle}{\omega_{kg} - \omega} \qquad (5)$$

It should be noted here that the definition of the two-photon transition matrix element tensor $\mathbf{M}_{fg}^{(2)}$ in this paper is somewhat different from the one used previously.[18,19] In eq 5, both ground

TPA Properties of 2D π-Conjugated Chromophores

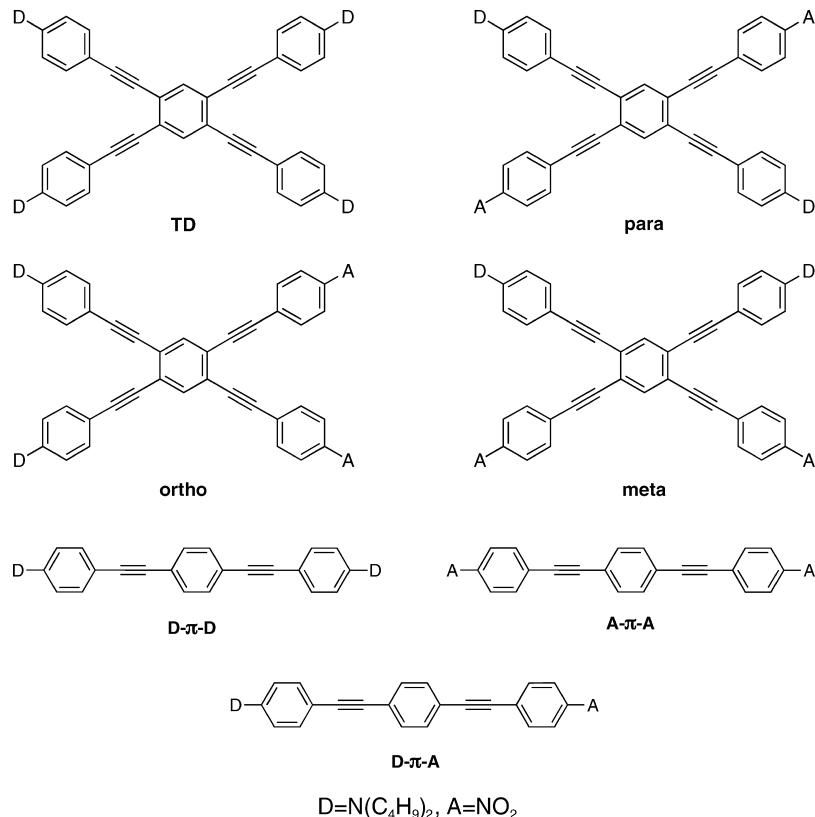*J. Phys. Chem. A, Vol. xxx, No. xx, XXXX* **C**

Figure 2. Molecular structures of TPEBs and the parent BPEBs studied.

($k = g$) and final ($k = f$) states are included in the summation as the intermediate state for noncentrosymmetric systems. In this case, eq 5 can be divided into two terms as

$$\mathbf{M}_{fg}^{(2)} = \frac{2}{\hbar}\left[\sum_{\substack{k \neq g \\ k \neq f}} \frac{\langle f|\vec{\varepsilon}\cdot\vec{\mu}|k\rangle\langle k|\vec{\varepsilon}\cdot\vec{\mu}|g\rangle}{\omega_{kg} - \omega} + \frac{(\vec{\varepsilon}\cdot\Delta\vec{\mu}_{fg})\langle k|\vec{\varepsilon}\cdot\vec{\mu}|g\rangle}{\omega}\right] \tag{6}$$

where $\Delta\vec{\mu}_{fg}$ is the difference between the dipole moments of the excited and ground states: $\Delta\vec{\mu}_{fg} = \langle f|\vec{\mu}|f\rangle - \langle g|\vec{\mu}|g\rangle$. In the derivation of eq 6, the two-photon resonance condition, $\omega_{fg} = 2\omega$, is used. The first summation term in eq 6 is called the three-state term, which appears in any system irrespective of the symmetry property, and the last term is called the dipolar term, which disappears in the centrosymmetric systems.

The orientationally averaged TPA probability $\langle|\mathbf{M}_{fg}^{(2)}|^2\rangle$ can be expressed for the linearly polarized incident light as

$$\langle|\mathbf{M}_{fg}^{(2)}|^2\rangle = \frac{1}{15}\sum_{\beta}^{x,y,z}\sum_{\alpha}^{x,y,z}(M_{\alpha\alpha}M_{\beta\beta}{}^* + 2M_{\alpha\beta}M_{\alpha\beta}{}^*) \tag{7}$$

where $M_{\alpha\beta}$ is each component ($\alpha, \beta = x, y, z$) of the two-photon transition matrix element and is expressed in terms of the corresponding component of the dipole transition moments as

$$M_{\alpha\beta} = \frac{1}{\hbar}\left[\sum_{\substack{k \neq g \\ k \neq f}}\left(\frac{\langle f|\mu_\alpha|k\rangle\langle k|\mu_\beta|g\rangle}{\omega_{kg} - \omega} + \frac{\langle f|\mu_\beta|k\rangle\langle k|\mu_\alpha|g\rangle}{\omega_{kg} - \omega}\right) + \left(\frac{\Delta\mu_{fg}{}^\alpha\langle f|\mu_\beta|g\rangle}{\omega} + \frac{\Delta\mu_{fg}{}^\beta\langle f|\mu_\alpha|g\rangle}{\omega}\right)\right] \tag{8}$$

where $\Delta\mu_{fg}{}^\alpha$ is each component of $\Delta\vec{\mu}_{fg}$. In the case of the noncentrosymmetric systems, from the division in eq 6, the orientationally averaged TPA probability $\langle|\mathbf{M}_{fg}^{(2)}|^2\rangle$ can be divided into the following three terms as

$$\langle|\mathbf{M}_{fg}^{(2)}|^2\rangle = \langle\mathbf{M}_{fg}^{(2)}\mathbf{M}_{fg}^{(2)*}\rangle = T_{\text{three-state}} + T_{\text{dipolar}} + T_{\text{cross}} \tag{9}$$

where

$$T_{\text{three-state}} = \frac{4}{15\hbar^2}\left[\sum_{\substack{k \neq g \\ k \neq f}}\sum_{\substack{k' \neq g \\ k' \neq f}}\frac{1}{(\omega_{kg} - \omega)(\omega_{k'g} - \omega)} \times \right.$$
$$\{(\langle f|\vec{\mu}|k\rangle\cdot\langle k|\vec{\mu}|g\rangle)(\langle f|\vec{\mu}|k'\rangle\cdot\langle k'|\vec{\mu}|g\rangle) + $$
$$(\langle f|\vec{\mu}|k\rangle\cdot\langle k'|\vec{\mu}|g\rangle)(\langle f|\vec{\mu}|k'\rangle\cdot\langle k|\vec{\mu}|g\rangle) + $$
$$\left.(\langle f|\vec{\mu}|k\rangle\cdot\langle f|\vec{\mu}|k'\rangle)(\langle k|\vec{\mu}|g\rangle\cdot\langle k'|\vec{\mu}|g\rangle)\}\right] \tag{10}$$

D *J. Phys. Chem. A, Vol. xxx, No. xx, XXXX*

Ohta et al.

$$T_{\text{dipolar}} = \frac{4}{15\hbar^2}\left[\frac{1}{\omega^2}\{|\Delta\vec{\mu}_{fg}|^2|\langle f|\vec{\mu}|g\rangle|^2 + \right.$$

$$\left. 2(\Delta\vec{\mu}_{fg}\cdot\langle f|\vec{\mu}|g\rangle)^2\}\right] = \frac{4}{15\hbar^2}\left[\frac{|\Delta\vec{\mu}_{fg}|^2|\langle f|\vec{\mu}|g\rangle|^2}{\omega^2}\times \right.$$

$$\left. (1 + 2\cos^2\phi)\right] \quad (11)$$

$$T_{\text{cross}} = \frac{8}{15\hbar^2}$$

$$\left[\sum_{\substack{k\neq g\\k\neq f}}\frac{1}{\omega(\omega_{kg}-\omega)}\{(\langle f|\vec{\mu}|k\rangle\cdot\langle k|\vec{\mu}|g\rangle)(\Delta\vec{\mu}_{fg}\cdot\langle f|\vec{\mu}|g\rangle)+\right.$$

$$(\langle f|\vec{\mu}|k\rangle\cdot\langle f|\vec{\mu}|g\rangle)(\Delta\vec{\mu}_{fg}\cdot\langle k|\vec{\mu}|g\rangle) +$$

$$\left. (\langle f|\vec{\mu}|g\rangle\cdot\langle k|\vec{\mu}|g\rangle)(\Delta\vec{\mu}_{fg}\cdot\langle f|\vec{\mu}|k\rangle)\}\right] \quad (12)$$

where ϕ is the angle between the two vectors $\Delta\vec{\mu}_{fg}$ and $\langle f|\vec{\mu}|g\rangle$. Here $T_{\text{three-state}}$ and T_{dipolar} are the three-state term and the dipolar term at the level of the TPA probability, respectively, each coming from the products within the first terms of eq 6 and the products of the last term of eq 6, respectively. T_{cross} is the cross term between the first and last terms of eq 6. In the actual TPA spectral simulation, a damping constant Γ_{kg} is incorporated in the denominator of the first summation of eq 8, as $\omega_{kg} - \omega \rightarrow \omega_{kg} - \omega - i\Gamma_{kg}$. For the normalized shape function $g(2\omega)$, the Lorentzian function is again used:

$$g(2\omega) = \frac{1}{\pi}\frac{\Gamma_{fg}}{(\omega_{fg}-2\omega)^2 + \Gamma_{fg}^2} \quad (13)$$

In previous studies,[18] a diagonal approximation was used in which the cross term between the three-state and dipolar terms of eqs 6 and 8 and also the products between the three-state terms having different intermediate states ($k \neq k'$) in the calculation of eq 10 were neglected; T_{cross} is then neglected, and $T_{\text{three-state}}$ is expressed as

$$T_{\text{three-state}} = \frac{4}{15\hbar^2}\left[\sum_{\substack{k\neq g\\k\neq f}}\frac{|\langle f|\vec{\mu}|k\rangle|^2|\langle k|\vec{\mu}|g\rangle|^2}{(\omega_{kg}-\omega)^2}(1 + 2\cos^2\theta_k)\right]$$

$$(14)$$

where θ_k is the angle between the two vectors $\langle f|\vec{\mu}|k\rangle$ and $\langle k|\vec{\mu}|g\rangle$. In the present study, however, this approximation was eliminated, and full calculations were carried out because we have found that the cross term of eq 12 often contributes significantly to the resultant TPA cross-section, as will be shown later.

For discussing the quantitative influence of the one-photon resonance on the TPA intensity in the three-state terms, the two quantities, $T_{\text{three-state}}(\omega_{fg}/2)$ and $T_{\text{three-state}}(0)$, are introduced. Here $T_{\text{three-state}}(\omega_{fg}/2)$ expresses the $T_{\text{three-state}}(\omega)$ value at the two-photon resonance condition, $\omega = \omega_{fg}/2$, expressed as a function of the frequency of the incident light. On the other hand, $T_{\text{three-state}}(0)$ expresses the value at the zero frequency and should be considered as the static limit of $T_{\text{three-state}}(\omega)$. The ratio $R_f^{(2)}$ of the two quantities is introduced as an index representing the influence of the one-photon resonance on the TPA intensity for each TPA allowed state. Using the $R_f^{(2)}$ value, the three-state term of the TPA probability may be expressed as the product of effect of resonance and pure transition moment factor

$$T_{\text{three-state}}(\omega_{fg}/2) = R_f^{(2)}T_{\text{three-state}}(0) \quad (15)$$

Employing the $R_f^{(2)}$ value, important electronic excited states that are the origin of double resonance can be specified. The $R_f^{(2)}$ value is approximately equal to the square of the ratio R_f between the scalar component of the transition polarizability tensor and its static value previously introduced[17] when only one component of the two-photon transition matrix element tensor is significantly large.

The molecules analyzed by calculation are shown in Figure 2. The experimental TPA properties of **TD** and **para** have been reported by Slepkov et al.[12] In the calculations, the dibutylamino groups are replaced with dimethylamino groups, as done previously.[10] The validity of this approximation is based on previous findings that symmetrically substituted stilbenes with amino groups having alkyl chains longer than methyl groups do not give TPA cross sections significantly different from that with dimethylamino groups.[18b] The molecular geometries used for the present calculations were the same as those previously optimized for the ground state of each molecule, which were obtained with the 6-31G(d) basis set by the DFT method with B3LYP parametrizations using the Gaussian program package.[23] The geometry data are available in the Supporting Information of ref 10. The optimized molecular structures belong to the point symmetry groups D_{2h}, C_i, C_s, and C_{2v}, for **TD**, **para**, **ortho**, and **meta**, respectively. While the structures of **para** and **ortho** deviate overall from C_{2h} and C_{2v} symmetry, respectively, the deviation is very small. Thus, the structures in ref 10 were used without any modification, but in discussing the symmetry property, the point groups C_{2h} and C_{2v} are assumed for **para** and **ortho**, respectively, for convenience.

All excited state properties including the TPA properties were calculated by the TDDFT/B3LYP method with the same 6-31G(d) basis set using both the Gaussian 03 program[24] and the DALTON 2.0 program[22] for the same geometries optimized for the ground states. It is known that the Gaussian program has somewhat different parametrization for the B3LYP functional from that in DALTON 2.0,[25] but the resultant excited state property is almost the same. For example, the difference in the excitation energies is within 0.01 eV, so it is valid to equate both parametrizations for convenience. The TPA properties can be calculated by two methods using the DALTON 2.0 program.[26] One is to calculate the second-order transition moments (keyword TWO-PHOTON) and the other is to calculate the transition moments between the excited states (keyword DOUBLE RESIDUE), both of which are based on the quadratic response calculations (keyword QUADRA). The former method calculates directly each component of the two-photon transition matrix element $\mathbf{M}_{fg}^{(2)}$ at two-photon resonance condition, $\omega = \omega_{fg}/2$. However, it is difficult to describe the dispersion behavior around the one-photon resonance in the TPA spectral simulation and to use the values for further analysis such as decomposition into each contributing term as in eq 9 or calculation of the static limit of the three-state term as $T_{\text{three-state}}(0)$. Therefore, for the TPA spectral simulation, the latter method was mainly employed, and each component of the two-photon transition matrix element was calculated using the sum-over-state formula within the limited number of the excited states. For this purpose, the lowest 34 excited states were taken
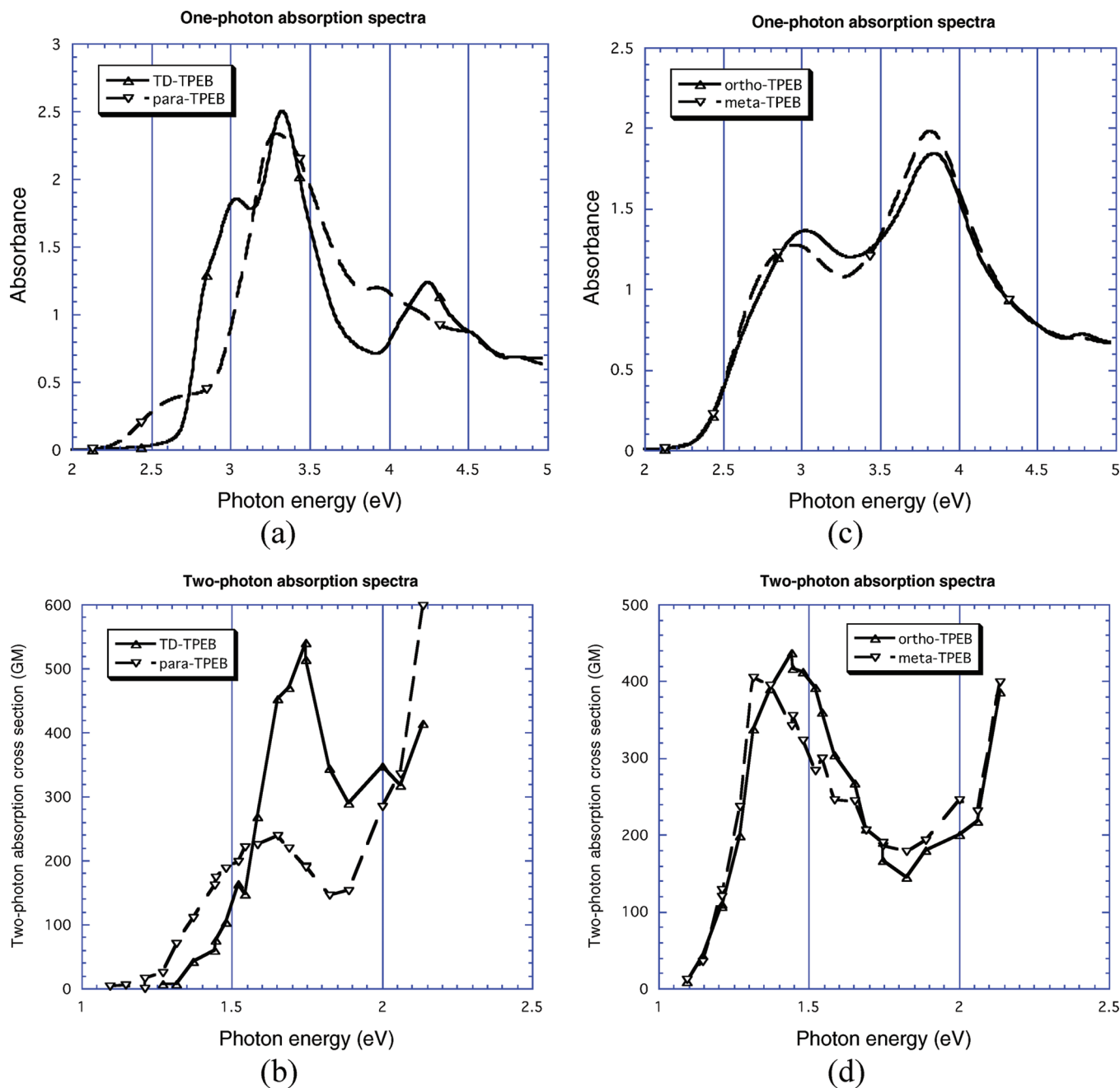
TPA Properties of 2D π-Conjugated Chromophores

J. Phys. Chem. A, Vol. xxx, No. xx, XXXX **E**

Figure 3. The experimental (a) OPA and (b) TPA spectra of the centrosymmetric TPEB, all-donor **TD** and **para**, and (c) OPA and (d) TPA spectra of the noncentrosymmetric TPEB, **ortho** and **meta**.

into account for **TD** and the lowest 20 excited states for the other molecules. For these spectra, this choice is sufficiently robust since these states cover the whole range of the photon energy of incident light used experimentally. The higher excited states can contribute to the TPA spectra as the intermediate states in eq 6 or 8. The contribution of such states is not expected to be large because of anticipated small transition moments with the ground state. The validity of this choice is checked through the comparison between the calculated values of each component of $\mathbf{M}_{fg}^{(2)}$ using the above two procedures.

3. Results and Discussion

3.1. Experimental OPA and TPA Spectra of TPEBs. *a. Centrosymmetric TPEBs.* Figure 3a shows the experimental OPA spectra of **TD** and **para** in THF. **TD** has the largest absorption peak at 3.32 eV in the OPA spectrum. The second

largest absorption peak is observed at 3.04 eV with a shoulder at 2.80 eV. A final band is observed at higher energy at 4.25 eV. The OPA spectrum of **para** has the largest peak at 3.29 eV, which is very close to that of **TD**, with a broad, weak shoulder around 2.5 eV. At the higher energy side, a weak absorption band is observed around 3.9 eV, which is less distinct than that of **TD**.

Figure 3b shows the experimental TPA spectra of these samples. **TD** is found to have a strong TPA band centered at 1.75 eV ($\Delta E = 3.49$ eV) with a cross-section of 520 GM. At the higher energy region, another less distinct TPA band is observed at 2.0 eV ($\Delta E = 4.0$ eV). On the other hand, **para** has a single low-energy TPA band centered at 1.65 eV ($\Delta E = 3.31$ eV). It should be noted that the peak cross-section for **para** (240 GM) is much smaller than that of **TD** (520 GM). Moreover, a large enhancement of TPA cross-section is observed at the

TABLE 1: Assignment of the Main Observed OPA and TPA Bands of TPEBs

	experimental		calculated		
	ΔE, eV (λ, nm)[a]	TPA cross sections $\sigma^{(2)}$ (GM)	ΔE (eV)	symmetry	orbital picture[b]
			TD		
OPA	2.80 (443) sh		2.68	$S_1(B_{2u})$	H (b_{2g}) → L (a_u) (0.93)
	3.04 (408)		2.90	$S_2(B_{3u})$	H − 1 (b_{3g}) → L (a_u) (0.88), H (b_{2g}) → L + 1 (b_{1u}) (0.44)
	3.32 (373)		3.26	$S_4(B_{3u})$	H (b_{2g}) → L + 1 (b_{1u}) (0.85), H − 1 (b_{3g}) → L (a_u) (−0.38)
	4.25 (292)		4.26	$S_{16}(B_{3u})$	H − 5 (b_{3g}) → L (a_u) (0.89)
TPA	3.49 (710)*	520	3.45	$S_5(A_g)$	H − 3 (a_u) → L (a_u) (0.93)
			3.86	$S_8(A_g)$	H − 2 (b_{1u}) → L + 1 (b_{1u}) (0.91)
	4.00 (620)*	340	4.05	$S_9(B_{1g})$	H − 3 (a_u) → L + 1 (b_{1u}) (0.98)
			4.18	$S_{14}(A_g)$	H − 1 (b_{3g}) → L + 2 (b_{3g}) (0.75)
			4.51	$S_{25}(A_g)$	H (b_{2g}) → L + 7 (b_{2g}) (0.62), H − 1 (b_{3g}) → L + 2 (b_{3g}) (0.51)
			4.60	$S_{26}(B_{1g})$	H − 1 (b_{3g}) → L + 7 (b_{2g}) (0.89)
			para		
OPA	2.5 (500) sh		1.87	$S_1(B_u)$	H (b_g) → L (a_u) (0.97)
			2.64	$S_4(B_u)$	H − 1 (a_u) → L + 1 (b_g) (0.99)
	3.29 (377)		2.87	$S_5(B_u)$	H (b_g) → L + 2 (a_u) (0.71), H − 2 (b_g) → L (a_u) (0.63)
			2.93	$S_6(B_u)$	H − 2 (b_g) → L (a_u) (0.70), H (b_g) → L + 2 (a_u) (−0.63)
	3.9 (320) wk		3.29	$S_8(B_u)$	H (b_g) → L + 3 (a_u) (0.77), H − 3 (b_g) → L (a_u) (−0.54)
			3.42	$S_{10}(B_u)$	H − 3 (b_g) → L (a_u) (0.80), H (b_g) → L + 3 (a_u) (0.55)
TPA	3.31 (750)*	240	3.21	$S_7(A_g)$	H − 2 (b_g) → L + 1 (b_g) (0.77), H − 1 (a_u) → L + 2 (a_u) (0.59)
			3.34	$S_9(A_g)$	H − 1 (a_u) → L + 2 (a_u) (0.73), H − 2 (b_g) → L + 1 (b_g) (−0.56)
	>4.24 (856)*	>600	3.76	$S_{14}(A_g)$	H − 3 (b_g) → L + 1 (b_g) (0.80), H − 1(a_u) → L + 3 (a_u) (−0.55)
			ortho		
OPA	3.03 (409)		2.37	$S_3(A_1)$	H − 1 (a_2) → L (a_2) (0.82), H (b_1) → L + 1 (b_1) (0.51)
	3.84 (323)		3.39	$S_9(A_1)$	H − 3 (a_2) → L (a_2) (0.68), H (b_1) → L + 3 (b_1) (−0.62)
TPA	2.88 (860)*	420	2.37	$S_3(A_1)$	H − 1 (a_2) → L (a_2) (0.82), H (b_1) → L + 1 (b_1) (0.51)
	>4.24 (856)*	>400	3.98	$S_{19}(A_1)$	H − 5 (a_2) → L (a_2) (0.98)
			meta		
OPA	2.96 (420)		2.38	$S_3(B_2)$	H (a_2) → L + 1 (b_1) (0.70), H − 1 (b_1) → L (a_2) (−0.66)
	3.81 (325)		3.32	$S_9(B_2)$	H − 2 (a_2) → L + 1 (b_1) (0.82), H − 3 (b_1) → L (a_2) (−0.49)
TPA	2.64 (940)*	400	2.18	$S_1(A_1)$	H (a_2) → L (a_2) (0.93)
			2.38	$S_3(B_2)$	H (a_2) → L + 1 (b_1) (0.70), H − 1 (b_1) → L (a_2) (−0.66)
			2.42	$S_4(A_1)$	H − 1 (b_1) → L + 1 (b_1) (0.97)
	>4.24 (856)*	>400	3.91	$S_{15}(B_2)$	H − 4(b_1) → L (a_2) (0.93)

[a] sh = shoulder, wk = weak. Excitation energy and the corresponding wavelength of the incident light. The photon energy is doubled for the excitation energy of a TPA bands (shown with *). [b] H and L stand for HOMO and LUMO, respectively. Value in the parentheses is the coefficient of each electronic configuration.

higher energy region up to the measurement limit (2.12 eV, ΔE = 4.24 eV), as described previously.[12]

In the case of the centrosymmetric molecules **TD** and **para**, the parity selection rule holds. Therefore, it is valid to consider that the OPA and TPA result in the excited states having different origins, even if OPA and TPA allowed states are present at energy levels near to each other. These spectroscopic parameters are summarized in Table 1 with the tentative assignments of the main OPA and TPA bands for all four TPEBs, which will be discussed in the later sections.

b. Noncentrosymmetric TPEBs. Figure 3c shows the experimental OPA spectra of **ortho** and **meta** in THF. As seen in the figures, the OPA spectra of **ortho** and **meta** are very similar to each other in peak positions, intensities, and spectral shapes. This is also true for the TPA spectra (Figure 3d). The largest OPA peaks are observed, respectively, at 3.84 and 3.81 eV for **ortho** and **meta** with the second largest peaks located around 3.03 and 2.96 eV. In the TPA spectra, **ortho** has a peak at 1.44 eV (ΔE = 2.88 eV), whereas **meta** has a peak at 1.32 eV (ΔE = 2.63 eV), with almost the same magnitude of the cross-section (420 and 400 GM, respectively). At a photon energy higher than 2.0 eV, both spectra show enhancement in the TPA cross-section. These spectroscopic parameters are also summarized in Table 1.

It is worth noting that the shape of the OPA and TPA spectra differs considerably from each other, even though the TPA transitions occur to the same excited states where the OPA transitions occur because of the noncentrosymmetry of these molecules. This discrepancy is discussed in a later section with the assignment of the transitions.

3.2. Calculated OPA and TPA Spectra of TPEBs. Figure 4 shows the simulated (a) OPA and (b) TPA spectra of the two centrosymmetric TPEBs (**TD** and **para**) and the simulated (c) OPA and (d) TPA spectra of the two noncentrosymmetric TPEBs (**ortho** and **meta**). The simulations are made on the basis of eqs 1 and 4 for the OPA and TPA spectra, respectively, where all the damping constants $\hbar\Gamma$ in the equations are assumed to be 0.248 eV, which corresponds to a wavenumber of 2000 cm^{-1}, so as to reproduce the distinct nature of peaks in the observed spectra. Full numerical data calculated for the excited states used for the simulations are available in the Supporting Information, where Tables S1, S2, S3, and S4 show the calculated excitation energies, symmetry species, main contributing electronic configurations, oscillator strength, and TPA probability of the excited states of **TD**, **para**, **ortho**, and **meta**, respectively. Here the TPA probabilities $\langle|M_{fg}^{(2)}|^2\rangle$ calculated by the two methods mentioned above are listed. As mentioned previously, the calculated molecular structures of **para** and **ortho** can approximately be considered to have the C_{2h} and C_{2v} symmetry, respectively. Therefore, the irreducible representation in Tables S2 and S3 is described in terms of the C_{2h} and C_{2v} symmetry, respectively.

TPA Properties of 2D π-Conjugated Chromophores

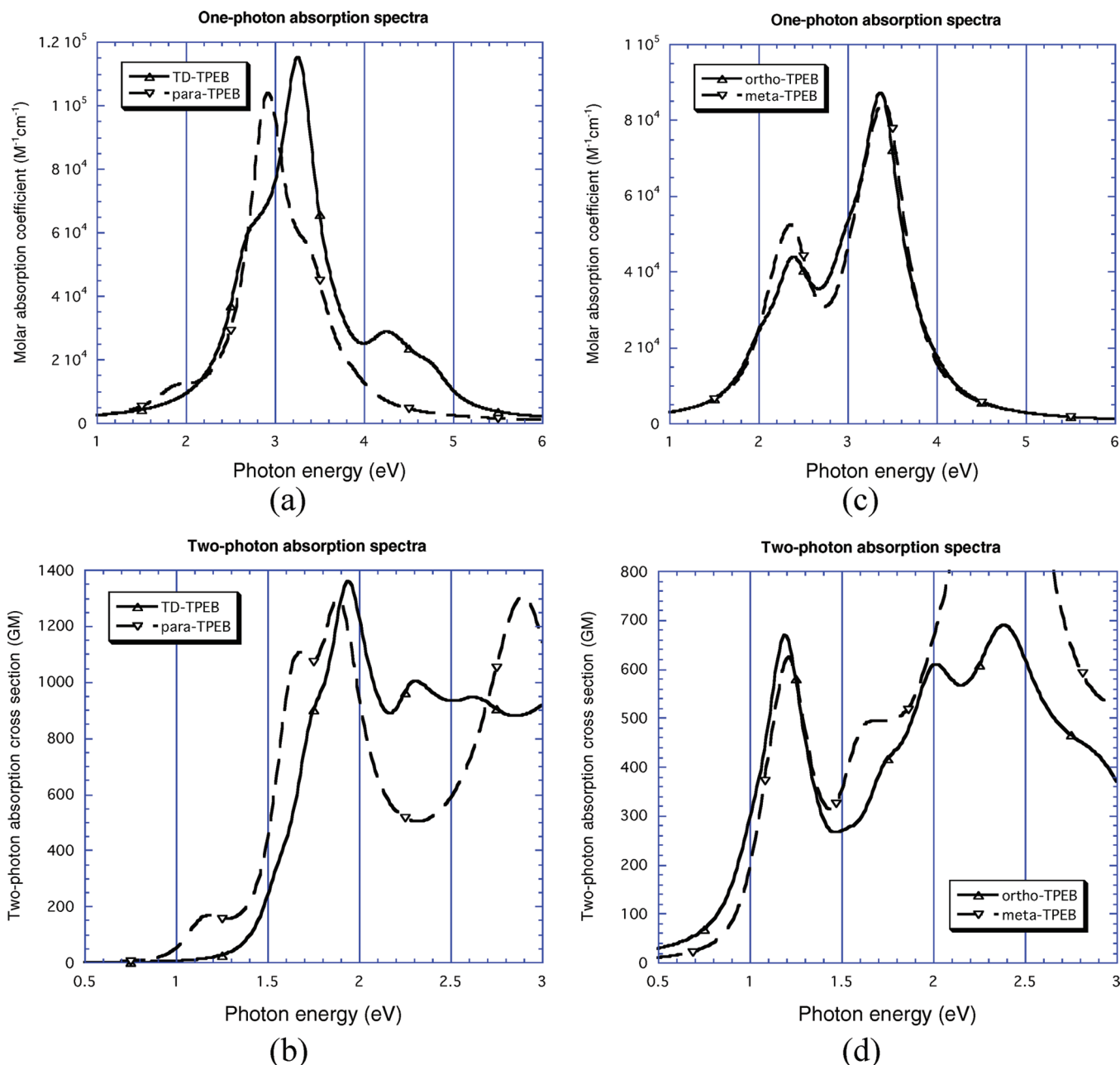*J. Phys. Chem. A, Vol. xxx, No. xx, XXXX* **G**

Figure 4. The simulated (a) OPA and (b) TPA spectra of the centrosymmetric TPEB, all-donor **TD** and **para**, and (c) OPA and (d) TPA spectra of the noncentrosymmetric TPEB, **ortho** and **meta**.

a. Centrosymmetric TPEBs. Figure 4a shows the calculated OPA spectra of **TD** and **para**. We can see that the calculated spectra simulate nicely most of the features found in the experimental spectra. For **TD**, not only the largest peak in 3.0−3.5 eV with a broad shoulder at the lower energy region but also a small peak at 4.0 eV observed for the experimental spectra (Figure 3a) are successfully reproduced in the calculated spectrum. For **para**, an underestimation of about 0.4−0.6 eV is found in the calculated excitation energies. For example, the largest OPA peak appears at 2.93 eV in the calculation, which should correspond to the peak at 3.29 eV in the experiment. This underestimation may be due to the B3LYP parametrization used for the present TDDFT calculations. However, if this underestimation is taken into account, the calculated spectrum well-simulates the experimental one (Figure 3a) in the spectral shapes.

Figure 4b shows the calculated TPA spectra of **TD** and **para**. For **TD**, the largest TPA band at 1.5−1.9 eV and a broad

shoulder in the lower energy region (Figure 3b) are reproduced well in the simulated spectrum. Moreover, a smaller peak observed at 2.0 eV is also found in the calculated spectrum, although the calculated excitation energies are somewhat overestimated about 0.3 eV. For **para**, the TPA bands in 1.3−1.8 eV are well-reproduced in the calculated spectra, except the relative magnitude against that of **TD**. Moreover, the observed increase in the higher energy region of 1.8−2.2 eV also appears in the calculated spectrum. The relative magnitude of 1.3−1.8 eV bands for **para** against that of **TD** is much larger than observed experimentally. The reason of this is not yet clear; nevertheless, the calculated spectra reproduce the general features of the experimental TPA spectra.

b. Noncentrosymmetric TPEBs. Parts c and d of Figure 4 show the calculated OPA and TPA spectra, respectively, of **ortho** and **meta**. The calculated OPA and TPA spectra simulate well the experimentally observed spectra (Figure 3c,d) even for the noncentrosymmetric TPEBs, although the calculated excita-

tion energies are underestimated for both OPA and TPA spectra, which can reflect the common defect in the TD-B3LYP approximation for the CT systems. The relative magnitude of the spectra is well-reproduced not only for the OPA but also for the TPA spectra.

By using the similarity in the spectral shapes for both centrosymmetric and noncentrosymmetric TPEBs, we can make assignment and further interpretation of the main bands of experimental OPA and TPA spectra, which are summarized in Table 1.

3.3. Interpretation of the Experimental OPA and TPA Spectra Based on the Calculation Results. For further interpretation of the experimentally observed spectra, it is useful to discuss the spatial distribution of the molecular orbitals concerning OPA or TPA excitations, particularly in comparison to those of the constituent parts, $D-\pi-D$, $A-\pi-A$, and $D-\pi-A$ BPEBs (see Figure S1a–c, Supporting Information). Figure 5 shows the orbital maps of four occupied and four unoccupied π-orbitals near the HOMO and LUMO of (a) **TD**, (b) **para**, (c) **ortho**, and (d) **meta**. From the figures, it is clear that the TPEB MOs are derivable from linear combination of the MOs of the two crossing BPEB [bis(phenylethynyl)benzene] derivatives. This finding is quite useful for analysis of the observed OPA and TPA spectra, and hereafter, the respective BPEB derivatives will be called parent BPEBs. The degree of the mixing strongly depends on the configuration of peripheral donor or acceptor groups. In the centrosymmetric TPEBs, the symmetry properties of MO such as parity (gerade or ungerade) are preserved from the parent BPEBs. Figure 6a shows such mixing of the MOs near the HOMO and LUMO of the parent BPEBs of $D-\pi-D$ and $A-\pi-A$ types in the centrosymmetric TPEBs (**TD** and **para**). Figure 6b shows similar mixing of the MOs near the HOMO and LUMO of the parent BPEBs of $D-\pi-A$ types in the noncentrosymmetric TPEBs (**ortho** and **meta**).

a. Centrosymmetric TPEBs. **TD.** In the case of **TD**, the π-MOs near the HOMO or LUMO can be described by linear combinations of those of two equivalent parent BPEBs, as shown in Figure 6(a). In the parent BPEB, the MOs with gerade (g) and ungerade (u) character appear almost alternatively near the HOMO or LUMO, where the HOMO belongs to g symmetry (b_{2g} in the D_{2h} point group) and the LUMO to u symmetry (b_{1u} in D_{2h}). As the result of the orbital mixing of the two BPEB molecules, both HOMO − 1 and HOMO of **TD** have the g symmetry, where the HOMO − 1 belongs to b_{3g} and the HOMO to b_{2g}. Likewise, both LUMO and LUMO + 1 have the u symmetry, where the LUMO belongs to a_u and the LUMO + 1 to b_{1u}, as shown in the calculated orbital maps of **TD** in Figure 5a. The HOMO → LUMO transition in the parent BPEB is one-photon allowed and two-photon forbidden. Similarly, all transitions from HOMO − 1 (b_{3g}) or HOMO (b_{2g}) to LUMO (a_u) or LUMO + 1 (b_{1u}) are also one-photon allowed and two-photon forbidden for **TD**, which restricts both its OPA and TPA spectroscopic properties. For example, due to parity in the centrosymmetry, the appearance of the TPA allowed (g) states for **TD** are very sparse (as shown in Table S1, Supporting Information).

In the Supporting Information, tentative assignment of OPA and TPA bands and possible virtual transition paths of main TPA bands of **TD** are described in detail. On the basis of the assignment, it turns out that several mechanisms govern the intensities in the TPA bands characteristic to **TD** in addition to the parity selection rules. One is that among the two symmetry-allowed species, the states with the A_g symmetry show relatively

larger TPA intensity than those with the B_{1g} symmetry. For example, the observed TPA peak with the strong intensity at 1.75 eV is assigned to two excited A_g states, S_5 and S_8, which show larger TPA intensity than the S_3 state, which belongs to the B_{1g} symmetry. This is due to the factor of $1 + 2 \cos^2 \theta_k$ in eq 14. Another mechanism which governs the relative TPA intensity is a magnitude relation between the conjugate-pair in terms of the alternancy symmetry having the same spatial symmetry species, discussed in the previous paper.[18a] For example, the $S_5(A_g)$ and $S_8(A_g)$ states together should form a conjugate-pair, and usually, the TPA intensity becomes larger for one state and smaller for the other. However, in the present case, the two states show similar TPA intensity. It is found that, due to the breaking of the alternancy symmetry, the main transition path can be different between the two states. Moreover, it is probable that the different transition paths negatively contribute to the total transition moment for the $S_8(A_g)$ state. This can be regarded as an example of destructive interference between different transition channels as proposed by Cronstrand et al.[27]

Para. In case of **para**, there is a crossing of the $D-\pi-D$ and $A-\pi-A$ structures present in the parent BPEBs. Therefore, the MOs near the HOMO of **para** are similar to those of $D-\pi-D$ and the MOs near the LUMO are similar to those of $A-\pi-A$, as shown in Figure 6a. This can be confirmed from the comparison among the orbital maps of **para** (Figure 5b) and the parent BPEBs (Figures S1a,b, Supporting Information). The transitions within the $D-\pi-D$ or $A-\pi-A$ moieties are similar to those of the parent $D-\pi-D$ or $A-\pi-A$ molecules. In the Supporting Information, tentative assignment of OPA and TPA bands and possible virtual transition paths of main TPA bands of **para** are described in detail. In the case of **para**, besides the parity selection rules, the larger orbital overlaps, which lead to larger transition densities between the orbitals at each step of the transitions, are found to be more critical in determining the TPA intensities. As shown in Figure 5b, the orbitals tend to be localized on either of the $D-\pi-D$ or $A-\pi-A$ moieties. Therefore, transitions between the same type of moieties gives larger transition densities. For example, the excitations to the $S_7(A_g)$ and $S_8(A_g)$ states occur within the $D-\pi-D$ or $A-\pi-A$ moieties. The experimental TPA bands around 1.3−1.8 eV can be assigned to these states. However, there exist transitions from the $D-\pi-D$ to $A-\pi-A$ moieties in the relatively lower energy regions. This characteristic of excitations of **para** affects the spectroscopic properties of both OPA and TPA.

Centrosymmetric chromophore **para** thus shows excitations with variable composition, including transitions within the same $D-\pi-D$ or $A-\pi-A$ moieties, as well as transition between the different moieties. This can account for the presence of the shoulder band at low energy in the OPA spectrum and/or the broad nature of the bands in the TPA spectrum. On the other hand, the molecular structure of **TD** is highly symmetric, and the orbitals and the transition densities are highly delocalized. Therefore, there is no TPA band in the lower energy region and the delocalized transition density is considered to be concentrated on particular transition paths. This can be the origin of the larger TPA cross-section observed for **TD**. Overall, the origin of each band in OPA and TPA spectra for the two centrosymmetric TPEBs is successfully explained by the present calculations.

b. Noncentrosymmetric TPEBs. **Ortho** *and* **Meta.** Two noncentrosymmetric TPEBs (**ortho** and **meta**) can be considered to belong to the C_{2v} point group, where **ortho** and **meta** have
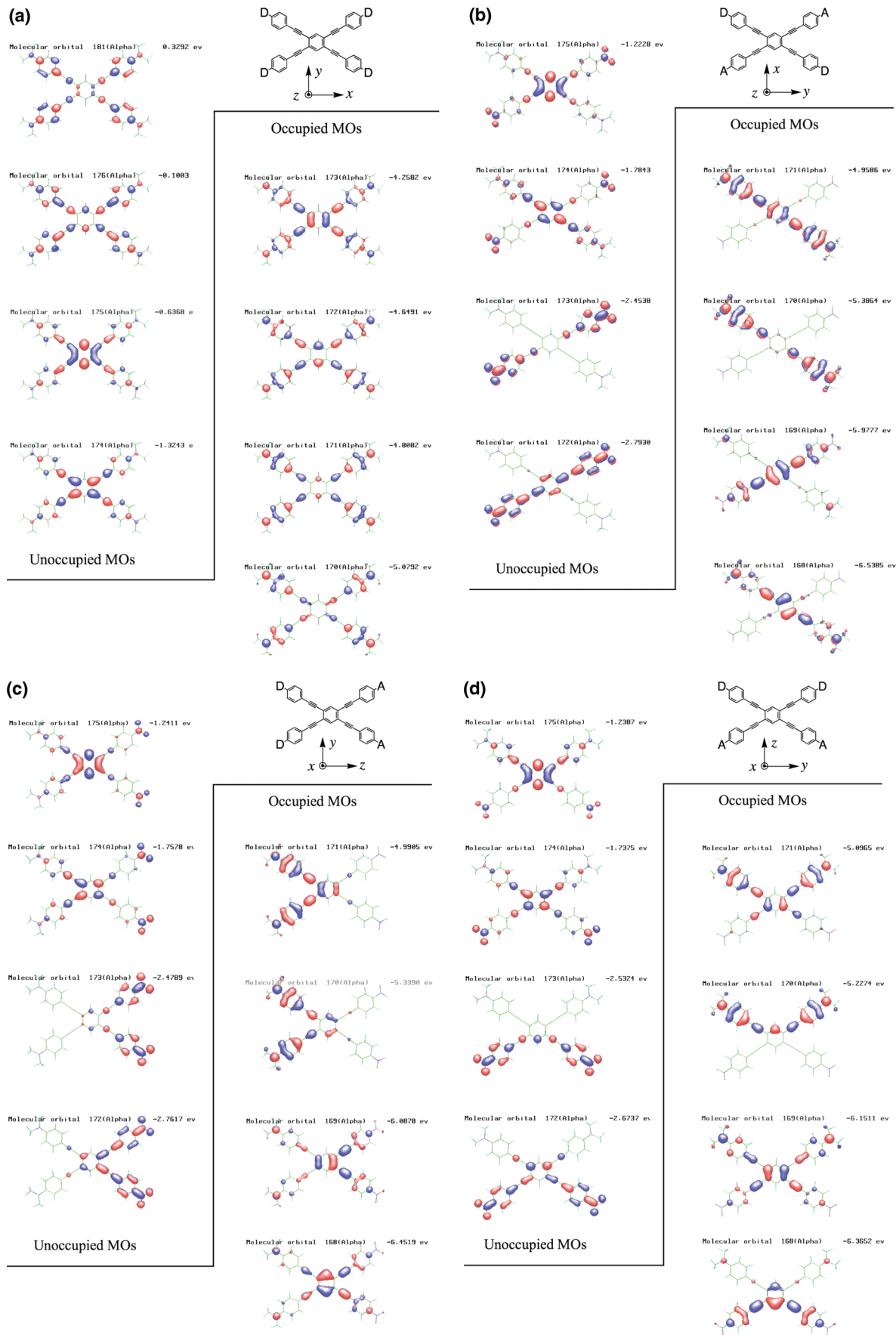
TPA Properties of 2D π-Conjugated Chromophores

J. Phys. Chem. A, Vol. xxx, No. xx, XXXX **I**

Figure 5. The orbital maps of π orbitals near the HOMO or LUMO of TPEBs calculated by the B3LYP method with the coordination systems: (a) **TD**, (b) **para**, (c) **ortho**, and (d) **meta**.
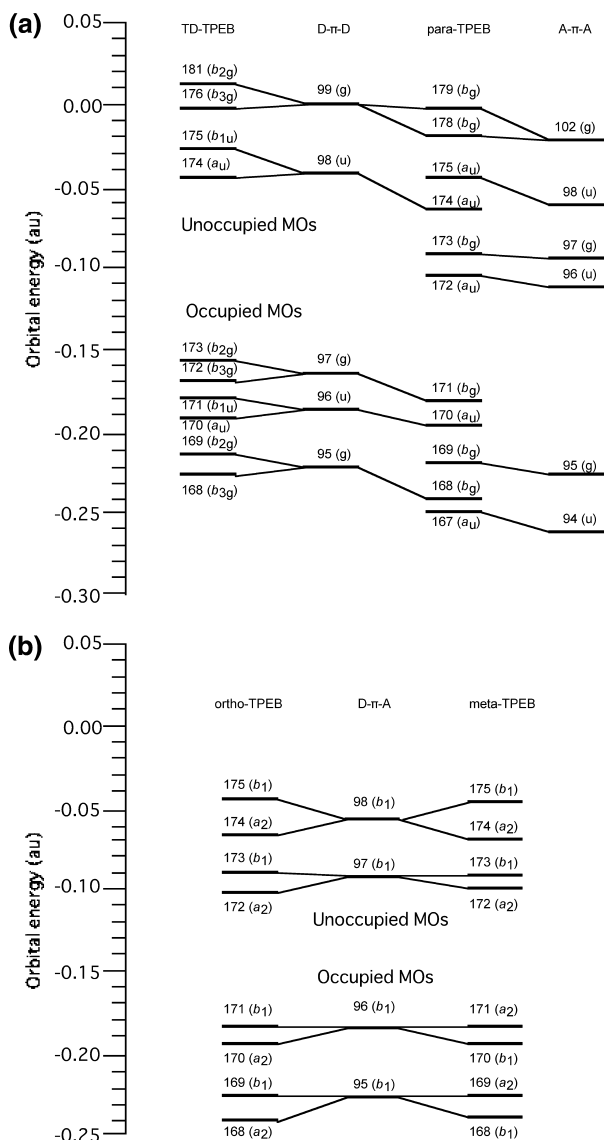
Figure 6. The orbital correlation diagrams of the MOs of parent BPEBs in (a) centrosymmetric TPEBs and in (b) noncentrosymmetric TPEBs.

the symmetry axis along the long and short axes of the molecules, respectively. In this point group, the excited states due to the $\pi-\pi^*$ excitation belongs to either of the A_1 or B_2 symmetry, both of which are, in principle, OPA- and TPA-allowed. Comparison of Tables S3 and S4 (Supporting Information) indicates that symmetry species of the lower excited states are different from each other. This originates from the fact that the ordering of the symmetry of the four orbitals from the HOMO − 3 to HOMO changes from a_2, b_1, a_2, and b_1 for **ortho** to b_1, a_2, b_1, and a_2 for **meta**, as shown in Figure 6b. This can be understood from the relationship of how the symmetries of the HOMO and LUMO of the central benzene ring are correlated with orbital symmetries in the different circumstance (e.g., in the C_{2v} point group with the different symmetry axis, as shown in Table S8, Supporting Information). For example, the lowest excited S_1 state belongs to B_2 for **ortho** and to A_1 for **meta**, and in both states, the main configurations correspond to the HOMO → LUMO transition. However, when the shape of molecule is considered as a rectangle, it is found that the directions of both transition moments are along the short axis of the rectangle. Thus, the common directions in the rectangular molecular shape rather than the common symmetry symbol are found to be primary responsible for the ordering of the excited

states. It is also found that the similarity in the OPA spectra between **ortho** and **meta** reflects the common direction of the transition moments in the molecular shape.

Contrary to the OPA properties, the difference between the A_1 or B_2 states becomes important for the TPA properties. For the molecules with the C_{2v} symmetry like **ortho** and **meta**, the A_1 excited states generally show stronger TPA intensities than the B_2 excited states. This results from the fact that for both of the three-state and dipolar terms in eq 9, the A_1 state shows three times intensity of the B_2 state when the permanent and transition dipole moment values are the same. This situation is summarized for C_{2v} symmetry in Table S5 (Supporting Information) and shows some differences in the TPA properties between **ortho** and **meta**, even though experimental and simulated TPA spectra appear similar to each other.

*c. Classification of Excited States of **Ortho** and **Meta**.* From the orbital pictures for the transitions to the lower $\pi-\pi^*$ excited states of **ortho** and **meta** shown in Tables S3 and S4 (Supporting Information), it is found that the excited states of the two TPEBs can be classified into two groups. One group is composed of the $S_1(B_2)$, $S_2(A_1)$, $S_3(A_1)$, and $S_4(B_2)$ states for **ortho** and the $S_1(A_1)$, $S_2(B_2)$, $S_3(B_2)$, and $S_4(A_1)$ states for **meta**, the transitions to which are the (HOMO − 1, HOMO) → (LUMO, LUMO + 1). The other group consists of the $S_5(B_2)$, $S_6(B_2)$, $S_7(A_1)$, $S_8(A_1)$, $S_9(A_1)$, $S_{10}(A_1)$, $S_{11}(B_2)$, and $S_{14}(B_2)$ states for **ortho** and the $S_5(A_1)$, $S_6(B_2)$, $S_7(A_1)$, $S_8(B_2)$, $S_9(B_2)$, $S_{10}(B_2)$, $S_{11}(A_1)$, and $S_{14}(A_1)$ states for **meta**, the transitions to which are due to the superposition of the (HOMO − 3, HOMO − 2) → (LUMO, LUMO + 1) transitions and the (HOMO − 1, HOMO) → (LUMO + 2, LUMO + 3) transitions, giving rise to the eight excited states in total. Furthermore, the excited states in each of the two groups do not mix electronic configurations (see Tables S3 and S4, Supporting Information).

This separation can be considered to be the result of linear combinations of MOs of the two identical noncentrosymmetric BPEB of the D−π−A type, as shown in Figure 6b for the TPEBs. The first group originates from the HOMO → LUMO transitions in the parent BPEB. Generally, the transition to the lowest excited state corresponds to the HOMO → LUMO transition having a strong intramolecular charge transfer (CT) character from the donor to acceptor groups for the polar molecules like the parent BPEB. The four lower excited states of the TPEBs also reflect such CT character. The second group originates from the HOMO → LUMO + 1 and HOMO − 1 → LUMO transitions in the parent BPEB.

On the basis of the classification above, a rough assignment of the OPA and TPA spectra can be made. The second largest OPA band at 2.9−3.1 eV in Figure 3c and the TPA band around 1.3−1.5 eV in Figure 3d can be due to the excited states in the first group. On the other hand, the largest OPA band at 3.8−3.9 eV can be due to the excited states in the second group. The corresponding TPA bands do not appear in the simulated spectra in spite of the strong OPA intensities. This is characteristic of the TPA spectra of the two molecules, and the mechanism of this diminishing intensity from OPA to TPA is discussed in the next subsection. As mentioned above, the mechanisms which govern the OPA intensities are similar to each other for **ortho** and **meta**, but those for the TPA intensity are slightly different. In the Supporting Information, tentative assignment of OPA and TPA bands for **ortho** and **meta** and differences in the mechanisms are described in detail.

*d. Destructive Interference in TPA Intensities of **Ortho** and **Meta**.* Next, the mechanism of diminishing intensities from OPA to TPA observed for the bands in the second group of the

TPA Properties of 2D π-Conjugated Chromophores

J. Phys. Chem. A, Vol. xxx, No. xx, XXXX **K**

noncentrosymmetric TPEBs, which show strong OPA but weak TPA intensities, is discussed. As discussed previously,[18b] two terms can contribute to the total TPA cross sections for the case of the noncentrosymmetric systems, that is, the dipolar and three-state terms shown in eq 6. The relative importance of the two terms can vary depending on the character of the excited states. The dipolar term becomes dominant when the state has a large transition moment with the ground state, which can be observed in the OPA intensities, and also large difference in the permanent dipole moments with the ground state. The three-state term becomes dominant when the transition moment between the ground and another intermediate excited state is large and the state itself has a large transition moment with the intermediate exited state. Resonance enhancement can be expected from the three-state term. In the lowest excited state, it is natural to consider that the dipolar term contributes much more than the three-state terms, because the intermediate state, which is necessary for the three-state term, always lies in the higher energy region for the lowest excited state and the energy denominator in the equation becomes larger. In fact, on the basis of this consideration, the TPA intensities for the lowest excited states in most noncentrosymmetric molecules have been discussed only with the dipolar terms. On the contrary, for the excited states other than the lowest state, both terms can contribute concurrently to the total TPA intensity.

There are several possibilities that lead to TPA intensity that are small despite large OPA intensities. One is the case where the difference in the permanent dipole moment with the ground state is small and the transition moments with other excited states are also small. Alternatively, the possibility can be considered where the cross term negatively contributes and the cancellation in total TPA intensity occurs, even if each term has sufficiently large values. Figure 7 shows the spectral simulation of the decomposition into the contributing terms including the cross term for the (a) **ortho** and (b) **meta**. Large negative values in the cross terms are observed in the region over 1.5 eV. It can also be seen in Tables S9 and S10 that, for the $S_9(A_1)$ and $S_8(A_1)$ states of **ortho** and for the $S_{10}(B_2)$ and $S_9(B_2)$ states of **meta**, large cancellation occurs to give small TPA intensities even though the three-state terms have large values. This can be regarded as another type of constructive or destructive interference between different transition channels.[27]

This kind of the interference effect was previously discussed by Delysse et al.[28] Following Delysse et al., when only one excited state (k) contributes as the intermediate state to the three-state term and, for example, all the transition moments are collinear, the TPA probability can be described by the following equation in the present formulation.

$$\langle|\mathbf{M}_{fg}^{(2)}|^2\rangle = \frac{4}{5\hbar^2}\left[\left|\frac{\langle f|\bar{\mu}|k\rangle\langle k|\bar{\mu}|g\rangle}{\omega_{kg}-\omega}\right| \pm \left|\frac{\Delta\bar{\mu}_{fg}\langle f|\bar{\mu}|g\rangle}{\omega}\right|\right]^2$$

(16)

This leads to a simple relationship among the amounts of the three terms as $T_{cross} = \pm\sqrt{T_{three\text{-}state}T_{dipolar}}$, where the sign is indicative of the constructive (+) or destructive (−) interferences. In fact, it can be seen in Tables S9 and S10 (Supporting Information) that some excited states of the two molecules approximately satisfy the relationship. The destructive interference effect can account for why the bands in the second group do not show large TPA cross sections in the experimental observations.
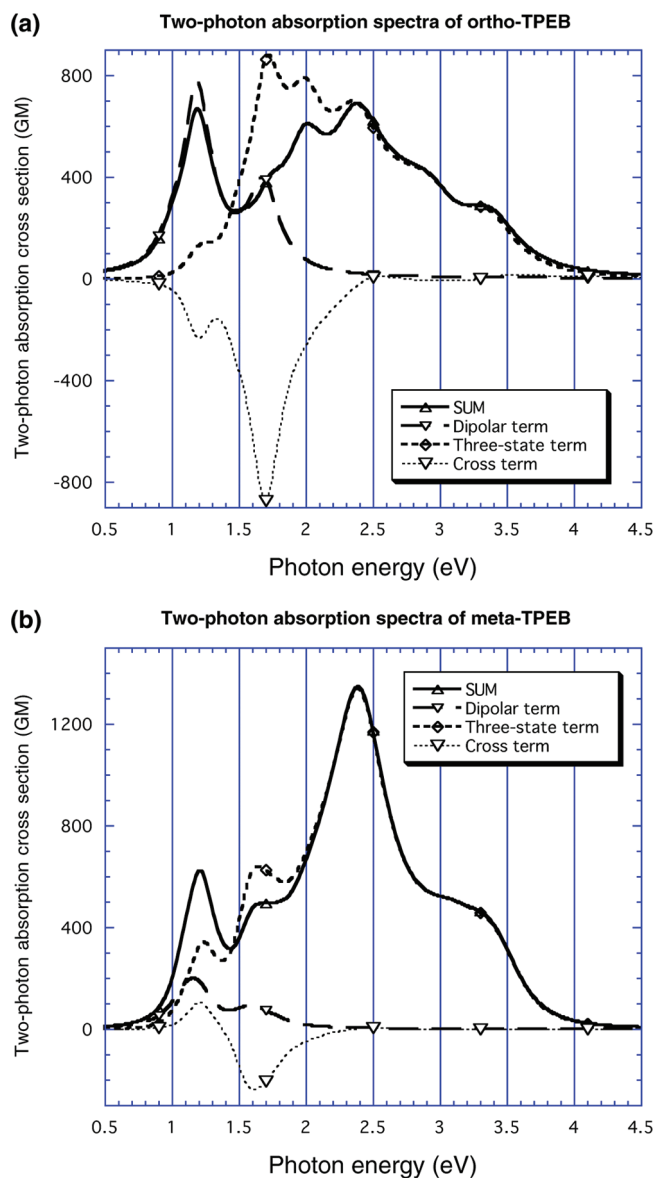
(a) Two-photon absorption spectra of ortho-TPEB

(b) Two-photon absorption spectra of meta-TPEB

Figure 7. Decomposition of the simulated TPA cross-section into the dipolar, three-state, and cross terms for (a) **ortho** and (b) **meta**.

Conclusions

In this paper, the results of our analysis on the TPA properties of model two-dimensionally extended π-conjugated TPEBs are reported by comparing each spectral band experimentally observed with those of the present MO calculations. The theoretical spectra simulated from the calculations reproduce well the experimental spectra observed not only for OPA but also for TPA. On the basis of the calculations, the origin of all spectral bands was specified at the levels of electronic configurations or orbitals. It is revealed that the TPA properties vary depending on the species or positions of the substituents for the two-dimensionally extended systems. The all donor substituted TPEB, **TD**, is highly symmetric, and MOs near the HOMO or LUMO are highly delocalized. This concentrates large transition densities on specific transition paths, which gives rise to larger TPA cross sections than other centrosymmetric systems, such as **para** TPEB. In **para**, different types of the transition paths are allowed. From these observations, it is found that the primary factor to control the TPA properties is the molecular symmetry. For the symmetric molecules, it is possible to control the TPA strength by adjusting of the molecular structure so as

L *J. Phys. Chem. A, Vol. xxx, No. xx, XXXX*

Ohta et al.

to concentrate the transition densities to some specific transition paths. The two noncentrosymmetric TPEBs, **ortho** and **meta**, show similar spectra in both OPA and TPA. However, the present analysis indicates that the origins of TPA can be different. The origin of the TPA spectra of **ortho**, which shows the transition moment along the long axis of the molecule for the important excited states, is more like that of one-dimensional D$-\pi-$A molecules. On the other hand, for **meta**, there exist the excited states specific to the two-dimensional molecules, in which the directions of the transition moment and the dipole moment are perpendicular to each other. Additionally, it should be pointed out that no TPA bands are observed that correspond to the strongest excited states observed in the experimental OPA spectra of the two TPEBs, **ortho** and **meta**, irrespective of the fact that all the excited states should be symmetry-allowed for both OPA and TPA transitions due to lack of the centrosymmetry. The present theoretical analysis reveals that this is due to the destructive interference between different transition paths with different characters. This phenomenon can be considered a sort of purely quantum mechanical effects, which are expected for processes concerning multiphoton transitions like TPA.[27,28] This finding may lead us to another way of controlling the TPA properties in the molecular systems, for example, enhancement of the TPA strength using the constructive interference among different transition paths.

Supporting Information Available: The detailed interpretation of the experimental results based on the theoretical calculations, the orbital maps of π-orbitals of parent BPEBs, and complete tables of the calculated results of the excited states of TPEBs are provided, as well as complete lists of authors of refs 22, 23, and 24. This material is available free of charge via the Internet at http://pubs.acs.org.

References and Notes

(1) (a) He, G. S.; Tan, L.-S.; Zheng, Q.; Prasad, P. N. *Chem. Rev.* **2008**, *108*, 1245–1330. (b) Rumi, M.; Barlow, S.; Wang, J.; Perry, J. W.; Marder, S. R. *Adv. Polym. Sci.* **2008**, *213*, 1–95. (c) Terenziani, F.; Katan, C.; Badaeva, E.; Tretiak, S.; Blanchard-Desce, M. *Adv. Mater.* **2008**, *20*, 4641–4678.

(2) Tykwinski, R. R.; Gubler, U.; Martin, R. E.; Diederich, F.; Bosshard, C.; Günter, P. *J. Phys. Chem. B* **1998**, *102*, 4451–4465.

(3) Rumi, M.; Pond, S. J. K.; Meyer-Friedrichsen, T.; Zhang, Q.; Bishop, M.; Zhang, Y.; Barlow, S.; Marder, S. R.; Perry, J. W. *J. Phys. Chem. C* **2008**, *112*, 8061–8071.

(4) Ren, Y.; Xin, Q.; Tao, X. T.; Wang, L.; Yu, X. Q.; Yang, J. X.; Jiang, M. H. *Chem. Phys. Lett.* **2005**, *414*, 253–258.

(5) Wang, L.; Tao, X. T.; Yang, J. X.; Xu, G. B.; Ren, Y.; Liu, Y.; Yan, Y. X.; Liu, Z.; Jiang, M. H. *Synth. Met.* **2006**, *156*, 141–145.

(6) He, F.; Tian, L.; Tian, X.; Xu, H.; Wang, Y.; Xie, W.; Hanif, M.; Xia, J.; Shen, F.; ang, B.; Li, F.; Ma, Y.; Yang, Y.; Shen, J. *Adv. Funct. Mater.* **2007**, *17*, 1551–1557.

(7) For other recent studies of nonlinear optical properties for multidimensional systems, see: (a) Kannan, R.; He, G. S.; Lin, T.-C.; Prasad, P. N.; Vaia, R. A.; Tan, L.-S. *Chem. Mater.* **2004**, *16*, 185–194. (b) Mongin, O.; Porrès, L.; Katan, C.; Pons, T.; Mertz, J.; Blanchard-Desce, M. *Tetrahedron Lett.* **2003**, *44*, 8121–8125. (c) Le Droumaguet, C.; Mongin, O.; Werts, M. H.; Blanchard-Desce, M. *Chem. Commun.* **2005**, 2802–2804. (d) Yoo, J.; Yang, S. K.; Jeong, M.-Y.; Ahn, H. C.; Jeon, S.-J.; Cho, B. R. *Org. Lett.* **2003**, *5*, 645–648. (e) Yang, W. J.; Kim, D. Y.; Kim, C. H.; Jeong, M.-Y.; Lee, S. K.; Jeon, S.-J.; Cho, B. R. *Org. Lett.* **2004**, *6*, 1389–1392. (f) Collings, J. C.; Poon, S.-Y.; Le Droumaguet, C.; Charlot, M.; Katan, C.; Palsson, L.-O.; Beeby, A.; Mosely, J. A.; Kaiser, H. M.; Kaufmann, D.; Wong, W.-Y.; Blanchard-Desce, M.; Marder, T. B. *Chem.—Eur. J.* **2009**, *15*, 198–208. (g) Kamada, K.; Antonov, L.; Yamada, S.; Ohta, K.; Yoshimura, T.; Tahara, K.; Inaba, A.; Sonoda, M.; Tobe, Y. *ChemPhysChem* **2007**, *8*, 2671–2677. (h) Katan, C.; Tretiak, S.; Werts, M. H. V.; Bain, A. J.; Marsh, R. J.; Leonczek, N.; Nicolaou, N.; Badaeva, E.; Mongin, O.; Blanchard-Desce, M. *J. Phys. Chem. B* **2007**, *111*, 9468–9483. (i) Kang, H.; Evmenenko, G.; Dutta, P.; Clays, K.; Song, K.; Marks, T. J. *J. Am. Chem. Soc.* **2006**, *128*, 6194–6205. (j) Woo, H. Y.; Hong, J. W.; Liu, B.; Mikhailovsky, A.; Korystov, D.; Bazan, G. C. *J. Am. Chem. Soc.* **2005**, *127*, 820–821.

(8) (a) Tolosa, J.; Zucchero, A. J.; Bunz, U. H. F. *J. Am. Chem. Soc.* **2008**, *130*, 6498–6506. (b) Hauck, M.; Schonhaber, J.; Zucchero, A. J.; Hardcastle, K. I.; Muller, T. J. J.; Bunz, U. H. F. *J. Org. Chem.* **2007**, *72*, 6714–6725. (c) Zucchero, A. J.; Wilson, J. N.; Bunz, U. H. F. *J. Am. Chem. Soc.* **2006**, *128*, 11872–11881.

(9) (a) Drobizhev, M.; Karotki, A.; Kruk, M.; Krivokapic, A.; Anderson, H.; Rebane, A. *Chem. Phys. Lett.* **2003**, *370*, 690–699. (b) Karotki, A.; Drobizhev, M.; Kruk, M.; Spangler, C.; Nickel, E.; Mamardashvili, N.; Rebane, A. *J. Opt. Soc. Am. B* **2003**, *20*, 321–332. (c) Ogawa, K.; Ohashi, A.; Kobuke, Y.; Kamada, K.; Ohta, K. *J. Am. Chem. Soc.* **2003**, *125*, 13356–13357. (d) Morisue, M.; Ogawa, K.; Kamada, K.; Ohta, K.; Kobuke, Y. *Chem. Commun.* **2010**, 2121–2123. (e) Ikeda, C.; Yoon, Z. S.; Park, M.; Inoue, H.; Kim, D.; Osuka, A. *J. Am. Chem. Soc.* **2005**, *127*, 534–535. (f) Karotki, A.; Drobizhev, a.; Dzenis, Y.; Taylor, P. N.; Andersonc, H. L.; Rebane, A. *Phys. Chem. Chem. Phys.* **2004**, *6*, 7–10. (g) Yoon, M.-C.; Noh, S. B.; Tsuda, A.; Nakamura, Y.; Osuka, A.; Kim, D. *J. Am. Chem. Soc.* **2007**, *129*, 10080–10081.

(10) Marsden, J. A.; Miller, J. J.; Shirtcliff, L. D.; Haley, M. M. *J. Am. Chem. Soc.* **2005**, *127*, 2464–2476.

(11) (a) Samori, S.; Tojo, S.; Fujitsuka, M.; Spitler, E. L.; Haley, M. M.; Majima, T. *J. Org. Chem.* **2008**, *73*, 3551–3558. (b) Spitler, E. L.; Haley, M. M. *Tetrahedron* **2008**, *64*, 11469–11474. (c) Spitler, E. L.; Monson, J. M.; Haley, M. M. *J. Org. Chem.* **2008**, *73*, 2211–2223. (d) Spitler, E. L.; Haley, M. M. *Org. Biomol. Chem.* **2008**, *6*, 1569–1576. (e) Samori, S.; Tojo, S.; Fujitsuka, M.; Spitler, E. L.; Haley, M. M.; Majima, T. *J. Org. Chem.* **2007**, *72*, 2785–2793. (f) Spitler, E. L.; Shirtcliff, L. D.; Haley, M. M. *J. Org. Chem.* **2007**, *72*, 86–96.

(12) Slepkov, A. D.; Hegmann, F. A.; Tykwinski, R. R.; Kamada, K.; Ohta, K.; Marsden, J. A.; Spitler, E. L.; Miller, J. J.; Haley, M. M. *Opt. Lett.* **2006**, *31*, 3315–3317.

(13) Sheik-Bahae, M.; Said, A. A.; Wei, T.-H.; Hagan, D. J.; van Stryland, E. W. *IEEE J. Quantum Electron.* **1990**, *26*, 760–769.

(14) Kamada, K.; Matsunaga, K.; Yoshino, A.; Ohta, K. *J. Opt. Soc. Am. B* **2003**, *20*, 529–537.

(15) Kamada, K.; Ohta, K.; Iwase, Y.; Kondo, K. *Chem. Phys. Lett.* **2003**, *372*, 386–393.

(16) Slepkov, A. D.; Marsden, J. A.; Miller, J. J.; Shirtcliff, L. D.; Haley, M. M.; Kamada, K.; Tykwinski, R. R.; Hegmann, F. A. *Proc. SPIE* **2005**, *5934*, 29–37.

(17) Rumi, M.; Ehrlich, J. E.; Heikal, A. A.; Perry, J. W.; Barlow, S.; Hu, Z.; McCord-Maughon, D.; Parker, T. C.; Röckel, H.; Thayumanavan, S.; Marder, S. R.; Beljonne, D.; Brédas, J.-L. *J. Am. Chem. Soc.* **2000**, *122*, 9500–9510.

(18) (a) Ohta, K.; Kamada, K. *J. Chem. Phys.* **2006**, *124*, 124303. (b) Ohta, K.; Antonov, L.; Yamada, S.; Kamada, K. *J. Chem. Phys.* **2007**, *127*, 084504.

(19) The two-photon transition matrix element tensor $\mathbf{M}_{fg}^{(2)}$ in eq 5 is sometimes called the transition polarizability[20] or (first-order) transition hyperpolarizability.[21] The right hand side of eq 5 is twice that used previously.[18] Instead, the numerical coefficient in the right hand side of eq 4 is changed from 16 to 4 so that the definition of the TPA cross-section $\sigma^{(2)}(\omega)$ remains unchanged for the single-beam experiments. Accordingly, the right hand side of eq 8 is also twice that used previously. By adopting this definition, the two-photon transition matrix element can be set back to the original definition of the transition polarizability.[20a] Moreover, the numerical values of the calculated two-photon transition matrix elements are identified with the elements of the $\mathbf{S}$ tensor in the output of DALTON 2.0[22] used in the present study provided that the atomic unit is used as the unit system.

(20) (a) Born, M.; Huang, K. *Dynamical Theory of Crystal Lattices*; Oxford University Press: Oxford, 2002; p 203. (b) Bonin, K. D.; Kresin, V. V. *Electric-Dipole Polarizabilities of Atoms, Molecules, and Clusters*; World Scientific: Singapore, 1997; p 22. (c) Long, D. A. *The Raman Effect*; Wiley: New York, 2002; p 53.

(21) (a) Hanna, D. C.; Yuratich, M. A.; Cotter, D. *Nonlinear Optics of Free Atoms and Molecules*; Springer: New York, 1979; p 75. (b) Butcher,

TPA Properties of 2D π-Conjugated Chromophores

J. Phys. Chem. A, Vol. xxx, No. xx, XXXX **M**

P. N.; Cotter, D. *The Elements of Nonlinear Optics*; Cambridge University Press: Cambridge, 1990; p 96.

(22) Angeli, C.; et al. *DALTON, release 2.0*, 2005.

(23) Frisch, M. J.; et al. *Gaussian 98, revision A.6*, Gaussian, Inc.: Pittsburgh, PA, 1998.

(24) Frisch, M. J.; et al. *Gaussian 03, revision B.05*; Gaussian, Inc.: Pittsburgh, PA, 2003.

(25) Yanai, T.; Tew, D. P.; Handy, N. C. *Chem. Phys. Lett.* **2004**, *393*, 51–57.

(26) (a) Sałek, P.; Vahtras, O.; Helgaker, T.; Ågren, H. *J. Chem. Phys.* **2002**, *117*, 9630–9637. (b) Sałek, P.; Vahtras, O.; Guo, J.; Luo, Y.; Helgaker, T.; Ågren, H. *Chem. Phys. Lett.* **2003**, *374*, 446–452.

(27) (a) Cronstrand, P.; Luo, Y.; Ågren, H. *Chem. Phys. Lett.* **2002**, *352*, 262–269. Erratum *Chem. Phys. Lett.* **2002**, *363*, 198. (b) Cronstrand, P.; Luo, Y.; Ågren, H. *J. Chem. Phys.* **2002**, *117*, 11102–11106.

(28) Delysse, S.; Raimond, P.; Nunzi, J.-M. *Chem. Phys.* **1997**, *219*, 341–351.